Multiple Second-Order Generalized Integrators Based Comb Filter for Fast Selective Harmonic Extraction

Chuan Xie, Kai Li and Jianxiao Zou
School of Automation Engineering,
Univ. of Elect. Sci. & Tech. of China
Chengdu, Sichuan 611731, China

Keliang Zhou
School of Engineering
University of Glasgow
Glasgow G12 8QQ, United Kingdom

Josep M. Guerrero
Department of Energy Technology
Aalborg University
Aalborg 9220, Denmark

***Abstract*—fast and accurate harmonic extraction plays a vital role in power quality assessment, grid synchronization, harmonic compensation, etc. This paper proposes a multiple second-order generalized integrators (SOGIs) based comb filter (SOGIs-CF) for fast selective harmonic extraction. Compared with the conventional multiple SOGI-quadrature signal generators (SOGI-QSGs) scheme, the tedious harmonic decoupling network (HDN) is removed off without sacrificing steady-state detection accuracy, and thus the computation burden can be reduced. In addition, the parameters design criteria and the digital implementation issues have been discussed in detail. Finally, the experimental results confirm the fast response and high detection accuracy of the proposed scheme. The characteristic of fast harmonic magnitude signal detection makes the proposed method quite suitable for the realization of flexible output capacity-limit control of multi-function inverters.**

***Keywords*—harmonic detection, second-order generalized integrator, quadrature signal generator, comb filter.**

I. INTRODUCTION

Harmonic-extraction has found wide applications in many occasions[1]–[5], such as power quality assessment devices, active power filters, grid synchronizations, etc. Various harmonic detection methods have been researched in the literature, which can be generally categorized into frequency-domain and time-domain methods [6].

Frequency-domain methods typically refer to the Fourier transform based techniques [7]–[11]. Discrete Fourier transform (DFT) methods transform time-domain signals to the frequency domain with prominent features like simplicity, selectivity, and high steady-state accuracy. The fast Fourier transform (FFT) implements the DFT in a modified form to reduce the computation burden and is widely used for harmonic monitoring and metering [6]. For real-time applications, the recursive DFT (RDFT) has gained wide interests in grid synchronization [7]–[9] and harmonic current compensation control [10]. The RDFT calculates a DFT on a sample-by-sample basis with the window shifting every sampling instant for a fixed number of samples, usually just one for simplicity. The major drawback of the above Fourier-based harmonic detection methods is the slow dynamic response and frequency sensitivity [6], [12]. Recently, an improved generalized DFT is proposed in to improve the dynamics and reduce the sensitivity to frequency variation [11]. However, the method depends on variable sampling frequency, which is not very suitable the system control, since it may change the dynamics of the system dynamics and particularly the plant model.

On the other hand, typical time-domain methods include, the instantaneous power theory (*pq* power theory) methods [13], second-order generalized integrator based quadrature signal generator (SOGI-QSG) based method [14], fundamental /harmonic-*dq*-frame methods [6], multiple-reference-frame (MRF) methods [15], adaptive notch filter (ANF) approaches [16], the cascaded-delayed-signal-cancellation (CDSC) techniques [12], the advanced Kalman-filter methods [17], etc. These time-domain methods can effectively extract the harmonic components, however, there exist some limitations. The *pq*-theory and fundamental-*dq*-frame-based techniques only estimate the fundamental signal and detect the rest harmonics as a whole, and are therefore incapable of selective harmonic extraction. The SOGI-QSG and the *dq*-frame-based methods need to make a tradeoff between steady-state accuracy and dynamics. The MRF-based, the ANF based, and the Kalman-filter-based approaches are essentially based on the concept of harmonic decoupling. Good accuracy and relatively fast dynamics can be achieved. However, all the harmonic components with non-negligible magnitudes must be estimated and extracted at the same time even though some of them are not desired. The CDSC-based methods can achieve relatively shorter transients with good accuracy. They are based on constructing a series of DSC operators, which consists of high-order delay buffers to separate the desired component and filter out the rest; therefore, for extracting each harmonic, different sets of DSC operators are required, which can increase the system complexity, computational effort, and storage memory overhead especially when many harmonic components are to be extracted in applications like the APF with selective harmonic compensation.

In this paper, a multiple resonators based comb filter is proposed for fast selective harmonic extraction. It is an improved scheme based on conventional SOGI-QSG schemes, which has advantages of the high steady-state accuracy, fast dynamic response, selectivity, frequency adaptation, and the reduced computation burden. Besides, it can also fast provides the harmonic magnitude information, which is quite suitable for harmonic compensation devices to realized flexible output capacity-limit control.

II. SYNTHESIS OF MULTIPLE SOGIS BASED COMB FILTER

A. the modified SOGI-QSG in s-domain

Fig. 1 shows the block diagram of the proposed modified SOGI-QSG rotated at h^{th} order harmonic. The transfer functions of the SOGI and the ones from the input signal v(s)

This work was supported by the National Natural Science Foundation of China under Grant 51807021 and 51707030, and the Sichuan Science and technology support program under Grant 2017GZ0051.

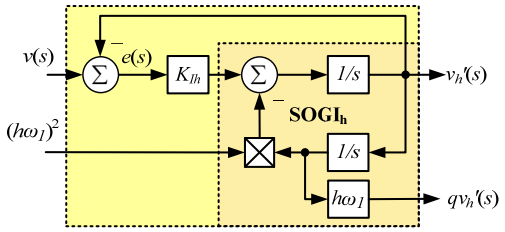

Fig. 1. Block diagram of the proposed modified SOGI-QSG rotated at h^{th} order harmonic.

to the output signal v'(s) and the corresponding orthogonal signal qv'(s) can be respectively expressed as

$$SOGI_h(s) = \frac{v_h'(s)}{e(s)} = \frac{K_{Ih}s}{s^2 + (h\omega_1)^2} \tag{1}$$

$$D_h(s) = \frac{v_h'(s)}{v(s)} = \frac{K_{Ih}s}{s^2 + K_{Ih}\cdot s + (h\omega_1)^2} \tag{2}$$

$$Q_h(s) = \frac{qv_h'(s)}{v(s)} = \frac{K_{Ih}h\omega_1}{s^2 + K_{Ih}\cdot s + (h\omega_1)^2} \tag{3}$$

where ω_1 is the fundamental angular frequency, h is the harmonic order, and K_{Ih} is the integral gain of the SOGI rotated as the frequency of $h\omega_1$.

The bode plots of D_h(s) and Q_h(s) with h =1 and $K_{I1}=\omega_1/2$ are given in Fig. 2. It can be seen from the figure that both of them exhibit the characteristic of BPF, and they both have the unit gains at the resonant frequency, meanwhile, there exist 0 and 90-degree delays at the at the resonant frequency for the D_h(s) and Q_h(s) respectively.

B. the proposed multiple SOGIs based comb filter

To accurately detect the sequence components of the grid voltage even under extreme distortion conditions, a cross-feedback network consisting of multiple SOGI-QSGs, as shown in Fig. 3, tuned at different harmonic frequencies, and working in a collaborative way is presented in [14]. It can be seen from the figure that a harmonic decoupling network (HDN) is used to isolate the effect of the different harmonics of the input signal.

To simplify the algorithm, a multiple SOGIs based comb filter (SOGIs-CF) scheme is proposed in this paper. The block diagram of the proposed SOGIs-CF is shown in Fig. 4.

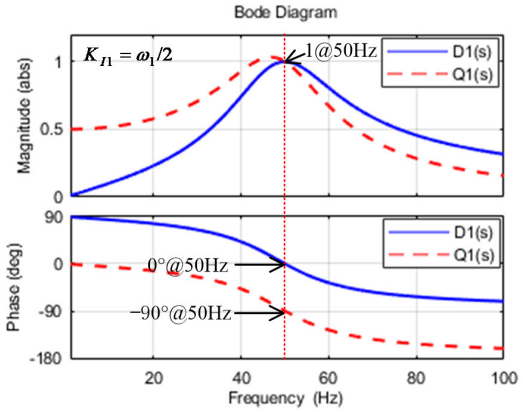

Fig. 2. Bode plots of D_h(s) and Q_h(s) with h =1 and $K_{I1}=\omega_1/2$.

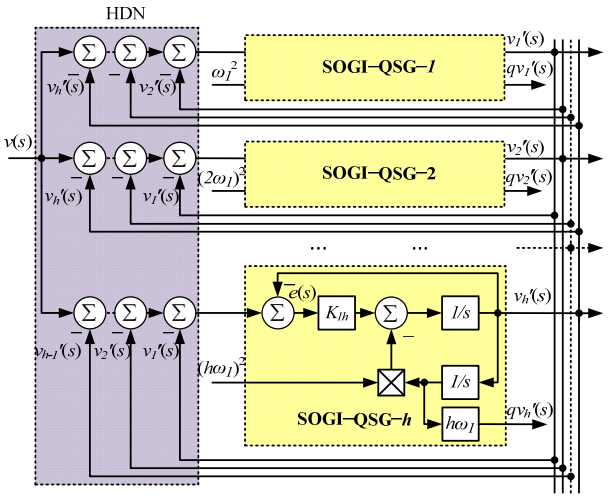

Fig. 3. Block diagram of the conventional multiple SOGI-QSGs scheme[14].

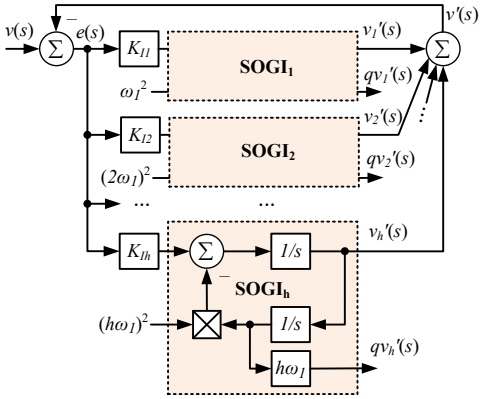

Fig. 4. Block diagram of the proposed multiple SOGIs based comb filter.

Compared with the conventional SOGI-QSGs [14], the tedious HDN can be removed off. If N sequence components of the input signal are extracted, $N\times N$ numbers of the subtraction operations can be reduced in the proposed SOGIs-CF scheme. The transfer functions from the input signal v(s) to the total output signal v'(s) and the individual signal v_h'(s) can be respectively expressed as

$$F(s) = \frac{v'(s)}{v(s)} = \frac{\sum_{h\in N_h} K_{Ih}\cdot SOGI_h(s)}{1+\sum_{h\in N_h} K_{Ih}\cdot SOGI_h(s)} \tag{4}$$

$$F_h(s) = \frac{v_h'(s)}{v(s)} = \frac{K_{Ih}\cdot SOGI_h(s)}{1+\sum_{h\in N_h} K_{Ih}\cdot SOGI_h(s)} \tag{5}$$

where N_h is the set of selected harmonic orders.

To achieve the high detection precision, all the harmonic components with non-negligible magnitudes must be taken into consideration and extracted at the same time even though some of them are not desired. Fig. 5 gives the bode plots of F(s), F_1(s) and F_3(s) with N_h= {1, 2, 3, 4, 5} for an example. It can be seen from the figure that every selected harmonic order component can be extracted out with zero steady-state error (unit gain and 0-degree phase lag at selected frequencies).

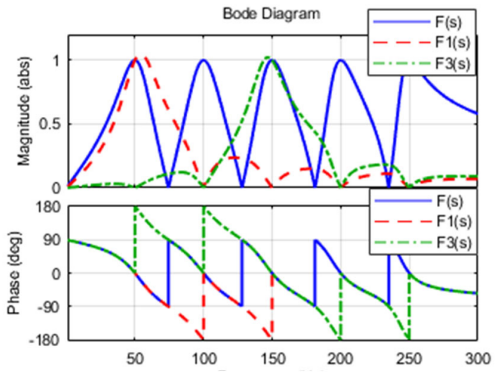

Fig. 5. Bode plot of $F(s)$, $F_1(s)$ and $F_3(s)$ with $N_h = \{1, 2, 3, 4, 5\}$.

C. Design of Parameters for SOGIs-CF

The proposed SOGIs-CF is apparently a closed-loop system, thus the system stability should be satisfied. The system stability can be checked via root locus of Eq. (4). Fig. 6 gives the root locus of $F(s)$ with $N_h = \{1, 2, 3, 4, 5\}$ for an example. It can be seen that the trajectory of the roots is always on the left half of the s-plane. Thus the SOGIs-CF closed-loop system is always stable no matter how much the proportional gain is.

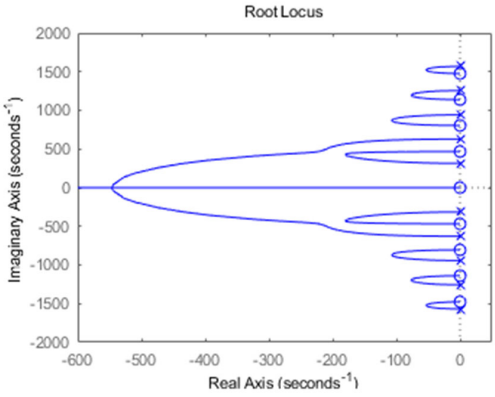

Fig. 6. Root locus of $F(s)$ with $N_h = \{1, 2, 3, 4, 5\}$.

To further choose the loop gain of the SOGIs-CF closed-loop system, the Laplace expression of the error signal $e(s)$, considering a single SOGI-QSG rotated at the fundamental angular frequency as the filter and a sine signal with the same angular frequency as the input signal, is derived as

$$e(s) = \overbrace{\frac{s^2+\omega_1^2}{s^2+K_{I1}\cdot s+\omega_1^2}}^{G_e(s)} \cdot \overbrace{\left(\frac{\omega_1\cos\varphi}{s^2+\omega_1^2}+\frac{s\cdot\sin\varphi}{s^2+\omega_1^2}\right)}^{L\{\sin(\omega_1 t+\varphi)\}} = \frac{\omega_1\cos\varphi + s\cdot\sin\varphi}{s^2+K_{I1}\cdot s+\omega_1^2} \quad (6)$$

Applying the inverse Laplace transformation to $e(s)$, the time-domain expression of the error signal $e(t)$ can be derived as follow.

$$e(t) = L^{-1}\{e(s)\} = \begin{cases} a_1 e^{-0.5K_{I1}t}\cos\omega_d t + b_1 e^{-0.5K_{I1}t}\sin\omega_d t & K_{I1} < 2\omega_1 \\ a_2 t e^{-\omega_1 t} + b_2 e^{-\omega_1 t} & K_{I1} = 2\omega_1 \\ a_3 e^{-\lambda_1 t} + b_3 e^{-\lambda_2 t} & K_{I1} > 2\omega_1 \end{cases} \quad (7)$$

where $a_1=\sin\varphi$, $b_1=[\cos\varphi\cdot\omega_1-\sin\varphi\cdot K_{I1}/2]/\omega_d$, $\omega_d=\sqrt{\omega_1^2-K_{I1}^2/4}$ $a_2=(\cos\varphi-\sin\varphi)\cdot\omega_1$, $b_2=\sin\varphi$, $a_3=(\omega_1\cdot\cos\varphi-\lambda_1\cdot\sin\varphi)/(\lambda_1-\lambda_2)$, $b_3=(\lambda_2\cdot\sin\varphi-\omega_1\cdot\cos\varphi)/(\lambda_1-\lambda_2)$, $\lambda_{1,2}=(K_{I1}\pm\sqrt{K_{I1}^2-4\omega_1^2})/2$.

According to the Eq. (7), the error signal convergence speed depends on not only the loop gain K_{I1} but also the input signal initial phase angle. Fig. 7 plots error signal convergence processes under different input signal initial phase angle φ and with loop gain equal to ω_1 or $4\omega_1$, respectively. The red contours indicate the locations where the magnitude of the error is attenuated to 10% of the initial value (It is the same meaning as in Fig. 8).

As can be seen from Fig. 7, when the initial phase angle $\varphi = 0$, the results are accurate enough to interpret the error signal convergence time in the case of $K_{I1} < \omega_1$ or $K_{I1} > \omega_1$. Thus, the effect of the SOGIs-CF closed-loop gain K_{I1} on the error signal convergence speed is evaluated under the condition of the initial phase angle $\varphi = 0$. Fig. 8 draws error signal convergence processes under different loop gains when the input signal initials phase angle $\varphi = 0$. It can be seen from Fig. 8 that relationship between the loop gain and the error signal convergence speed can be divided into three parts: 1) the loop gain is less than ω_1 or 2) larger than $4\omega_1$, the error signal convergence speed is proportional to the loop gain; 3) the loop gain is between ω_1 and $4\omega_1$, the error signal convergence speed is inverse proportional to the loop gain.

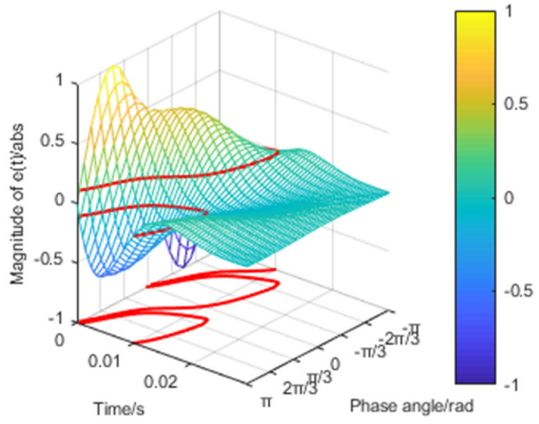

(a)

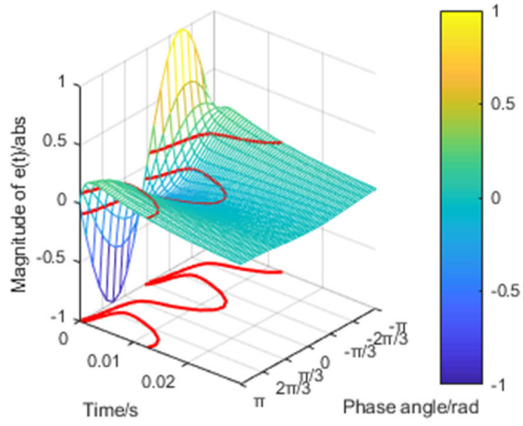

(b)

Fig. 7. Error signal convergence processes under different input singal initial phase angle φ with loop gain (a) $K_{I1} = \omega_1$ or (b) $K_{I1} = 4\omega_1$,.

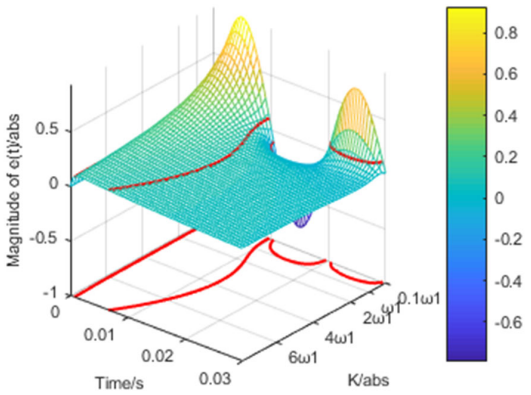

Fig. 8. Error signal convergence processes under different loop gains when the input singal inintial phase angle $\varphi = 0$.

Although the SOGIs-CF closed-loop system is always stable in the s-domain, too big loop gain is impractical and will destabilize the system since the digital implementation will introduce delay to the closed-loop system and deteriorate the system stable margin. To achieve fast dynamic response speed as well as enough stability margin, it's recommended that the loop gain should be set between ω_1 and $2\omega_1$.

D. Implementation of SOGI with two digital integrators

In order to obtain a pair of orthogonal signals, two *s*-domain integrators, as shown in Fig. 1, are discretized into z-domain with the forward Euler and backward Euler method [18], respectively. Fig. 9 shows the block diagram of the proposed modified SOGI-QSG rotated at h^{th} order harmonic with two digital integrators. According to Fig. 9, the z-domain transfer functions of the SOGI and the ones from the input signal $v(z)$ to the output signal $v'(z)$ and the corresponding orthogonal signal $qv'(z)$ can be respectively expressed as

$$SOGI_h(z) = \frac{v'_h(z)}{e(z)} = \frac{K_{Ih}T_s[\cos(h\omega_1 T_s)z - 1]}{z^2 - 2\cos(h\omega_1 T_s)z + 1} \quad (8)$$

$$D_h(z) = \frac{v'_h(z)}{v(z)} = \frac{K_{Ih}T_s[\cos(h\omega_1 T_s)z - 1]}{z^2 - (2 - K_{Ih}T_s)\cos(h\omega_1 T_s)z + 1 - K_{Ih}T_s} \quad (9)$$

$$Q_h(z) = \frac{qv'_h(z)}{v(z)} = \frac{K_{Ih}T_s[\cos(h\omega_1 T_s)z - 1]}{z^2 - (2 - K_{Ih}T_s)\cos(h\omega_1 T_s)z + 1 - K_{Ih}T_s} \quad (10)$$

where T_s is the sampling period.

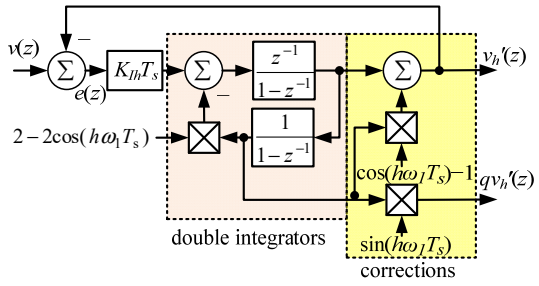

Fig. 9. Digital implementation of the proposed modified SOGI-QSG rotated at h^{th} order harmonic.

The bode plots of $D_h(z)$ and $Q_h(z)$ with $h = 1$, $K_{Il} = \omega_1/2$ and sampling frequency $f_s = 200$ Hz are given in Fig. 10. It can be seen from the figure that both of them exhibit the characteristic of BPF with unit gains and 0 and 90-degree delays at the at the resonant frequency respectively.

E. Magnitude information extraction with the SOGI-CF

In the conventional multiple SOGI-QSGs scheme, each SOGI-QSGs are in the parallel structure, thus each pair of orthogonal signals can be extracted by the corresponding SOGI-QSG individually. In the proposed SOGI-CF scheme, each SOGIs rotated at the different order harmonic frequencies construct their different QSGs via a same closed loop. Each pair of orthogonal signals concerning h^{th} order harmonic component still can be generated from the SOGIs rotated at the corresponding order harmonic frequency, thus the real-time magnitude of the extracted h^{th} order harmonic component, i.e., V_{hm}, can be calculated as follow.

$$V_{hm}(k) = \sqrt{v'_h(k)^2 + qv'_h(k)^2} \quad (11)$$

where k represents the discrete time signal index.

III. Experimental Results

To evaluate the performance of the proposed approach, the experimental testbed is built in the laboratory. The experimental testbed consists of one *Danfoss* converter connected to a three-phase diode rectifier through *LC* filters. The inverter serves as the grid emulator, and the rectifier emulates the nonlinear load. The hardware picture of the experimental setup is shown in Fig. 11.

In the proposed harmonic detection scheme, all the harmonic components with non-negligible magnitudes (N_h ={1, 5, 7, 11, 13, 17, 19} are extracted individually. The loop gain is set to $\sqrt{2}\omega_1$ and the sampling frequency is 10 kHz. The control algorithms are programmed in Matlab/Simulink and executed in a dSPACE controller board (DS1005). The experimental data are all saved by dSPACE ControlDesk.

Fig. 12 gives experimental results of the steady-state waveforms. Fig. 12(a) depicts that all extracted harmonic components via the proposed SOGIs-CF almost overlap with the input signal. This verifies the high steady-state measurement precision of the proposed method. Fig. 12(b) gives the waveforms of the fundamental and 5th harmonic components and the corresponding magnitude signals.

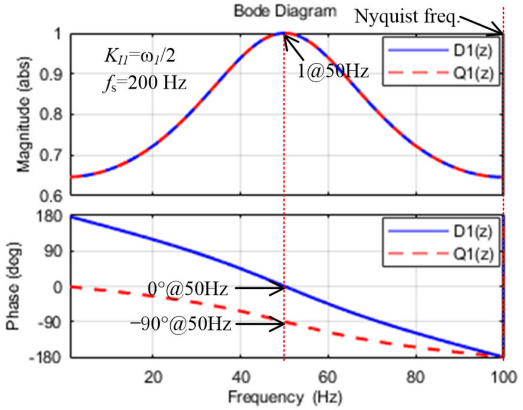

Fig. 10. Bode plot of $D_h(z)$ and $Q_h(z)$ with $h = 1$, $K_{Il}=\omega_1/2$, and $f_s = 200$ Hz.

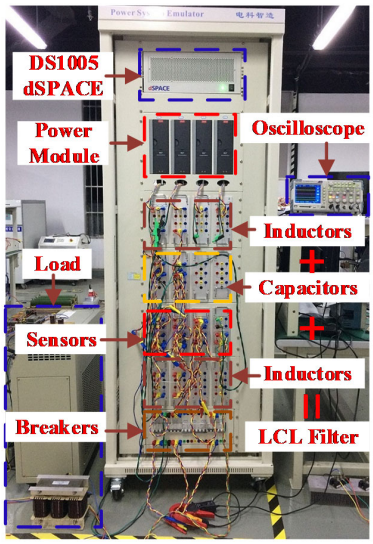

Fig. 11. Hardware picture for the experimental setup.

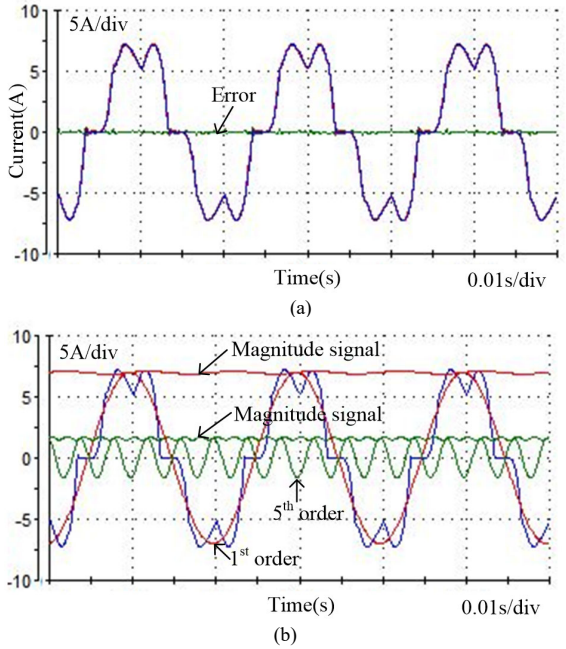

Fig. 12. Steady-state waveforms of (a) all and (b) individual harmonic components with the proposed SOGIs-CF.

Fig. 13 shows experimental results of all components extraction during wide range step change of grid frequency. Fig. 13(a) gives the waveforms of all components when the grid frequency steps up from 50Hz to 55Hz, while Fig. 13 (b) depicts the waveforms when the grid frequency steps down from 50Hz to 45Hz. It can be seen that the detection errors remains at a very low level in steady-state even the grid frequency fluctuates in a large range.

The transient experimental waveforms of all and individual harmonic components extraction are illustrated in Fig. 14 to evaluate the dynamic performance of the proposed method. It can be seen from Fig. 14 that it takes about the half cycle to reach the steady-state, which complies well with the theoretical analysis in Section II.C.

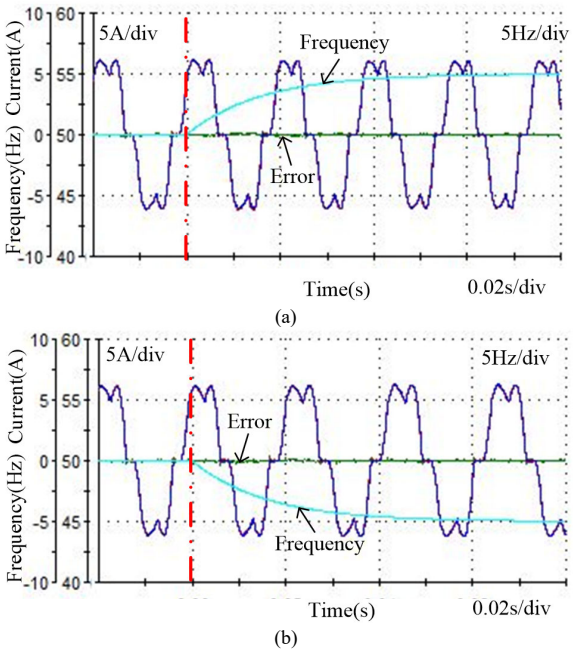

Fig. 13. Experimental results of all harmonic components extraction during wide (a) step up and (b)step down of the grid frequency.

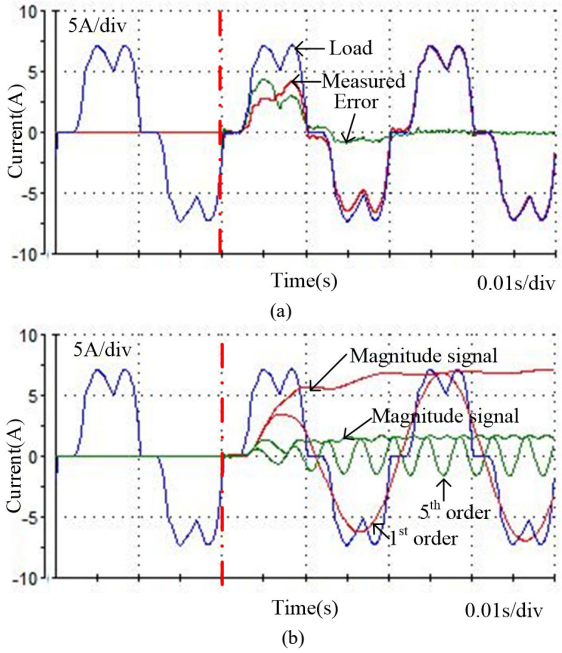

Fig. 14. The transient experimental waveforms of (a) all and (b) individual harmonic components extraction.

IV. CONCLUSIONS

In this paper, a multiple second-order generalized integrators based comb filter (SOGIs-CF) for fast selective harmonic extraction is proposed. Compared with the conventional multiple SOGI based bandpass filters (SOGI-QSGs), the tedious decoupling loop can be removed off without sacrificing steady-state detection accuracy, and thus the computation burden can be reduced. Besides, the characteristic of fast harmonic magnitude signal detection makes the proposed method quite suitable for the realization

of flexible output capacity-limit control of multi-function inverters. And the closed-loop system parameters design method is also discussed in the paper. Experimental results are provided to validate the theoretical expectations.

REFERENCES

[1] C. Xie, X. Zhao, M. Savaghebi, L. Meng, J. M. Guerrero, and J. C. Vasquez, "Multirate Fractional-Order Repetitive Control of Shunt Active Power Filter Suitable for Microgrid Applications," *IEEE Journal of Emerging and Selected Topics in Power Electronics*, vol. 5, no. 2, pp. 809–819, Jun. 2017.

[2] C. Xie, X. Zhao, K. Li, D. Liu, J. M. Guerrero, and J. C. Vasquez, "Phase Compensated Reduced Order Generalized Integrators for Grid-Tied VSCs With Harmonics Compensation Capability," *IEEE Transactions on Industry Applications*, vol. 54, no. 3, pp. 2568–2578, 2018.

[3] C. Xie, X. Zhao, K. Li, J. Zou, and J. M. Guerrero, "Multirate Resonant Controllers for Grid-Connected Inverters with Harmonic Compensation Function," IEEE Transactions on Industrial Electronics, p. 10. **DOI:** 10.1109/TIE.2018.2868249

[4] D. Liu, F. Deng, and Z. Chen, "Five-Level Active-Neutral-Point-Clamped DC/DC Converter for Medium-Voltage DC Grids," *IEEE Transactions on Power Electronics*, vol. 32, no. 5, pp. 3402–3412, May 2017.

[5] D. Liu, Y. Wang, F. Deng, Q. Zhang, and Z. Chen, "Zero-Voltage Switching Full-Bridge T-Type DC/DC Converter with Wide Input Voltage Range and Balanced Switch Currents," *IEEE Transactions on Power Electronics*, vol. 33, no. 12, p. 18, 2018.

[6] L. Asiminoaei, F. Blaabjerg, and S. Hansen, "Detection is key-Harmonic detection methods for active power filter applications," *Industry Applications Magazine, IEEE*, vol. 13, no. 4, pp. 22–33, 2007.

[7] F. A. S. Neves and M. C. Cavalcanti, "A Space-Vector Discrete Fourier Transform for Unbalanced and Distorted Three-Phase Signals," *IEEE Transactions on Industrial Electronics*, vol. 57, no. 8, pp. 2858–2867, Aug. 2010.

[8] F. A. S. Neves and F. Bradaschia, "Digital Filters for Fast Harmonic Sequence Component Separation of Unbalanced and Distorted Three-Phase Signals," *IEEE Transactions on Industrial Electronics*, vol. 59, no. 10, pp. 3847–3859, Oct. 2012.

[9] K. Duda, "Accurate, Guaranteed Stable, Sliding Discrete Fourier Transform," *IEEE Signal Process. Mag.*, vol. 27, no. 6, pp. 124–127, Nov. 2010.

[10] F. A. S. Neves, M. A. C. Arcanjo, G. M. S. Azevedo, H. E. P. de Souza, and L. T. Leon Viltre, "The SVFT-based control," *IEEE Transactions on Industrial Electronics*, vol. 61, no. 8, pp. 4152–4160, Aug. 2014.

[11] H. Liu, H. Hu, H. Chen, L. Zhang, and Y. Xing, "Fast and Flexible Selective Harmonic Extraction Methods Based on the Generalized Discrete Fourier Transform," *IEEE Transactions on Power Electronics*, vol. 33, no. 4, pp. 3484–3496, Apr. 2018.

[12] Y. F. Wang, "Three-Phase Cascaded Delayed Signal Cancellation PLL for Fast Selective Harmonic Detection," *IEEE Transactions on Industrial Electronics*, vol. 60, no. 4, pp. 1452–1463, Apr. 2013.

[13] F. Z. Peng, "Generalized Instantaneous Reactive Power Theory for Three-phase Power Systems," *IEEE Transactions on Instrumentation and Measurement*, vol. 45, no. 1, pp. 293–297, Feb. 1996.

[14] P. Rodriguez, A. Luna, I. Candela, R. Mujal, R. Teodorescu, and F. Blaabjerg, "Multiresonant Frequency-Locked Loop for Grid Synchronization of Power Converters Under Distorted Grid Conditions," *IEEE Transactions on Industrial Electronics*, vol. 58, no. 1, pp. 127–138, Jan. 2011.

[15] L. Hadjidemetriou and F. Blaabjerg, "A Robust Synchronization to Enhance the Power Quality of Renewable Energy Systems," *IEEE Transactions on Industrial Electronics*, vol. 62, no. 8, pp. 4858–4868, Aug. 2015.

[16] D. Yazdani, A. Bakhshai, and P. K. Jain, "A Three-Phase Adaptive Notch Filter-Based Approach to Harmonic/Reactive Current Extraction and Harmonic Decomposition," *IEEE Transactions on Power Electronics*, vol. 25, no. 4, pp. 914–923, Apr. 2010.

[17] A. Bagheri, M. Mardaneh, and A. Rajaei, "Detection of Grid Voltage Fundamental and Harmonic Components Using Kalman Filter and Generalized Averaging Method," *IEEE Transactions on Power Electronics*, vol. 31, no. 2, pp. 1064–1073, Feb. 2016.

[18] A. G. Yepes, F. D. Freijedo, J. Doval-Gandoy, Ó. López, J. Malvar, and P. Fernandez-Comesaña, "Effects of Discretization Methods on the Performance of Resonant Controllers," *IEEE Transactions on Power Electronics*, vol. 25, no. 7, pp. 1692–1712, Jul. 2010.